The relevance of electrostatics for scanning-gate microscopy

2011 New J. Phys. 13 053013

(http://iopscience.iop.org/1367-2630/13/5/053013)

New Journal of Physics
The open-access journal for physics

The relevance of electrostatics for scanning-gate microscopy

S Schnez[1], J Güttinger, C Stampfer[2], K Ensslin and T Ihn
Solid State Physics Laboratory, ETH Zürich, 8093 Zürich, Switzerland
E-mail: schnez@phys.ethz.ch

New Journal of Physics **13** (2011) 053013 (13pp)
Received 7 February 2011
Published 9 May 2011
Online at http://www.njp.org/
doi:10.1088/1367-2630/13/5/053013

Abstract. Scanning-probe techniques have been developed to extract local information from a given physical system. In particular, conductance maps obtained by means of scanning-gate microscopy (SGM), where a conducting tip of an atomic-force microscope is used as a local and movable gate, seem to present an intuitive picture of the underlying physical processes. Here, we argue that the interpretation of such images is complex and not very intuitive under certain circumstances: scanning a graphene quantum dot (QD) in the Coulomb-blockaded regime, we observe an apparent shift of features in scanning-gate images as a function of gate voltages, which cannot be a real shift of the physical system. Furthermore, we demonstrate the appearance of more than one set of Coulomb rings arising from the graphene QD. We attribute these effects to screening between the metallic tip and the gates. Our results are relevant for SGM on any kind of nanostructure, but are of particular importance for nanostructures that are not covered with a dielectric, e.g. graphene or carbon nanotube structures.

[1] Author to whom any correspondence should be addressed.
[2] Current address: JARA-FIT and II. Institute of Physics, RWTH Aachen, 52074 Aachen, Germany.

Contents

1. Introduction 2
2. Measurements 3
3. Discussion 5
4. Comparison with previous scanning-gate microscopy (SGM) experiments, summary 9
Acknowledgments 9
Appendix 10
References 12

1. Introduction

Scanning-gate microscopy (SGM) is a local probing technique that can unveil microscopic processes governing the conductance of nanostructures. The conducting tip of an atomic-force microscope is used to induce a potential perturbance in the nanostructure, thus altering the conductance of a particular sample as a function of tip position. Conductance maps are then obtained by recording the conductance while scanning the tip over the nanostructure. With this technique, various material systems and different types of nanostructures have been explored in the past, e.g. carbon nanotube-based quantum dots (QDs) [1], GaAs-based quantum-point contacts [2]–[4], quantum wires [5], InGaAs-bases quantum rings [6], GaAs-based QDs [7, 8], superconducting single-electron transistors [9] and recently graphene QDs [10].

Scanning a tip over nanostructures causes an unwanted effect: the electrostatic potential experienced by charge carriers in the nanostructure changes during a scan because the moving metallic tip partially screens the electric field emanating from gate electrodes. In other words, the mere presence of the tip alters the transport properties of a nanostructure, even if contact potential differences between tip and gates are compensated. Although this is an obvious effect, its importance has not been discussed in detail in the literature to our knowledge. Only in [1], where the authors vaguely attribute a conspicuous symmetry of the scanning-gate images to the electrostatic influence. However, they do not analyze their findings further.

With the advent of graphene, two aspects may increase the importance of these screening effects. Firstly, graphene samples are typically not covered with a dielectric and secondly, voltages up to several tens of volts are applied to lateral gates. In this paper, we will present SGM on a graphene QD sample. We will demonstrate that these screening effects can lead to apparent shifts of the QD resonances that are bigger than the lithographic extent of the sample. Moreover, under certain experimental conditions more than one set of Coulomb rings appears, which we also attribute to the strong screening effect. Our analysis will be corroborated with the constant-interaction model where we introduce the screening terms phenomenologically. We want to point out that our results are also of importance for other scanning-probe techniques, such as scanning-tunneling microscopy, although our findings are analyzed in the context of SGM.

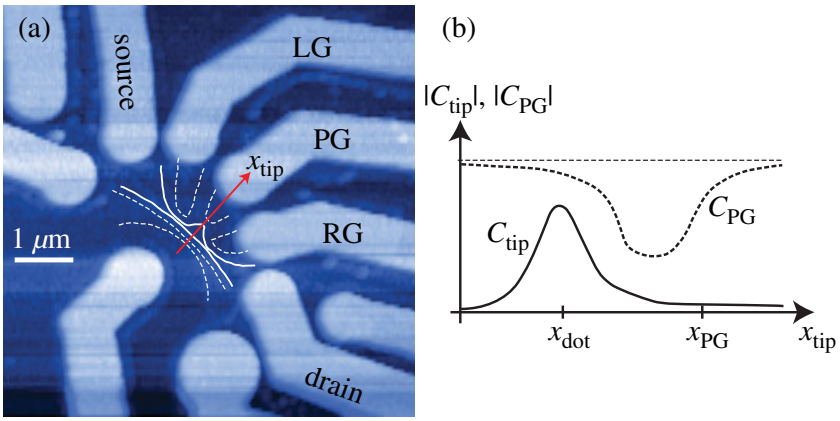

Figure 1. (a) Atomic-force micrograph of the graphene QD sample. Metallic electrodes contacting the gates and the QD are seen as bright areas. The (white) lines trace the edge of the different graphene structures, in particular the QD is traced with a continuous line. The tip-dot capacitance C_{tip} and the plunger gate-dot capacitance C_{PG} are considered at tip positions x_{tip} along the (red) arrow. In panel (b), we plot the qualitative evolution of these two values (absolute values) as a function of x_{tip}. For $x_{tip} \to \pm\infty$, $|C_{tip}|$ goes to zero, whereas $|C_{PG}|$ approaches a maximal value. $|C_{tip}|$ has a maximal value close to the dot. Due to screening by the tip, $|C_{PG}|$ is minimal somewhere between dot and gate position.

2. Measurements

We performed SGM on the same graphene QD that has already been discussed in [10]. The sample is shown in figure 1(a), where the bright areas are metallic gates contacting the graphene flake. The latter has been cut into the desired shape by reactive ion etching. The faint edges of the QD are retraced with continuous white lines between source and drain for better visibility of the structure. In-plane graphene gates (edges retraced with white dashed lines) used for tuning the device are denoted by 'LG', 'PG' and 'RG', standing for left, plunger and right gate, respectively. All other gates including the graphene nanoribbon (white, dashed lines to the lower left of the QD) were grounded throughout the experiment.

The QD has a lithographic radius of 110 nm and a charging energy of $\Delta E_C = 3.5$ meV. The charge neutrality point is around 30 V in back-gate voltage [10]. For a coherent set of data, we present only scanning-gate images obtained in the hole regime for back-gate voltages $V_{BG} \leqslant 25$ V. The temperature for the scanning-gate images presented here was between 2 and 2.6 K.

In figure 2(a), we present a scanning-gate image of the QD taken at $V_{BG} = 12$ V. Coulomb resonances of the QD show up as ring-shaped conductance resonances (in the following called *Coulomb rings*) and are centered around the (white) cross that may be interpreted as the location of the QD. The conductance is given in color code, where higher conductance is given by brighter, up to yellowish, colors. The strong, ring-like modulation of the Coulomb rings is due to localized states that are located in the constrictions. Their behavior has been analyzed previously [10]. Figure 2(b) presents the same scan frame, but with different voltages applied to the in-plane gates as denoted in the figure. The center of the Coulomb rings, again marked with a cross, shifts by about 110 nm.

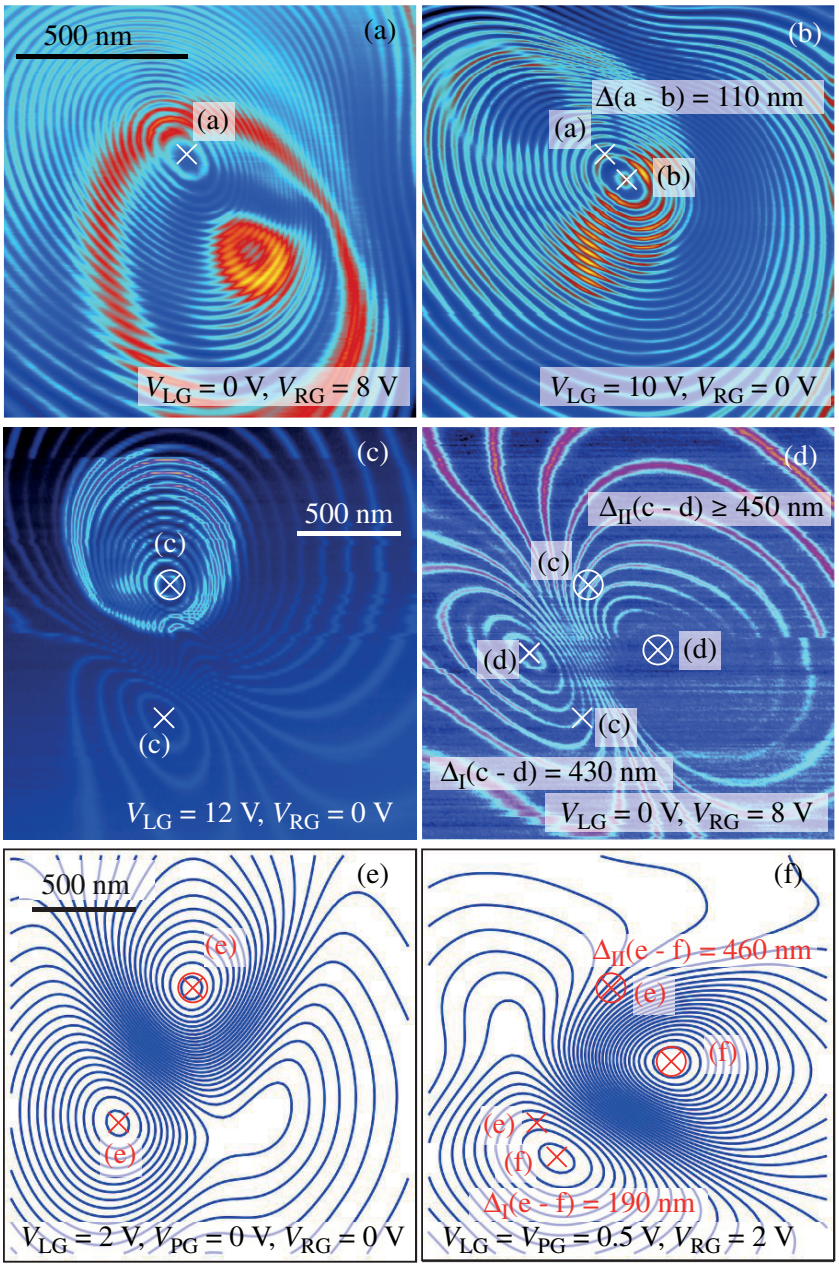

Figure 2. (a, b) Scanning-gate images taken in the hole regime for $V_{BG} = 12\,V$, $V_{tip} = 2\,V$ and $V_{bias} = 300\,\mu V$. The left- and right-side gates were changed as denoted in the figures. This results in an apparent shift of the centers of the Coulomb rings. These are denoted by (white) crosses; in (b) the center of (a) is also denoted. The overall shift is $\Delta = 110\,nm$. (c) and (d) Equivalent measurements as in (a) and (b) for $V_{BG} = 16\,V$. Two sets of Coulomb rings, which sense the same QD, are visible in this regime. By changing side-gate voltages, the centers of the two sets shift in opposite directions by in total $\Delta_I = 430\,nm$ for the lower and $\Delta_{II} \geqslant 450\,nm$ for the upper set. The center of the Coulomb rings in (d) for set II cannot be determined. Hence, just a lower bound for the total shift can be given. In all scanning-gate images, conductance is given in color code with

Figure 2. (Contd.) darker colors indicating lower conductance. (e) and (f) Numerical simulations of Coulomb resonances as imaged by SGM. A phenomenological screening term was introduced in the gate capacitances as described in the text. Then, the evaluation of the constant-interaction model leads to the appearance of two sets of Coulomb rings and a subsequent shift of their centers when different gate voltages are applied. Temperature and tunnel coupling broadening are not implemented in the model so that the Coulomb rings are arbitrarily sharp.

For a different back-gate voltage $V_{BG} = 16\,V$, we obtain qualitatively different images: figures 2(c) and (d) present two scanning-gate images where again in-plane gate voltages were changed as denoted in the images. We recognize two sets of Coulomb rings whose respective centers shift by 430 nm and more. This shift is significantly larger than the extent of the QD (diameter about 220 nm) and can therefore not be a real shift of the QD charge distribution.

In summary, we observe two unexpected effects, namely the appearance of more than one set of Coulomb rings and apparent shifts of their centers bigger than the extent of our device. For a correct interpretation of scanning-gate images, especially when we want to extract length scales, it is therefore crucial to understand where these two effects come from and how they can possibly be avoided in future experiments.

For a further analysis, we determined the centers of Coulomb rings of the QD and resonances of localized states in the constrictions for many scanning-gate images taken with this sample in the hole regime. The locations of all the centers are plotted in figure 3 with their corresponding error bars[3]. We distinguish the different resonances—Coulomb resonances of the QD or resonances of localized states in the constrictions—by using different symbols. The outline of the lithographic QD is shown as a black, dashed line to depict a reference for the geometry of the structure. Again, we see that the shifts observed in figure 3 cannot be accounted for by a shift in real space alone because they are much larger than the extent of the structure.

3. Discussion

There are three possible explanations for the observed shifts of Coulomb-ring centers, namely (i) a drift of the sample holder with respect to the tip over time, (ii) bending of the tip because of electrostatic forces between the tip and the surrounding and (iii) a change in the electrostatic fields and potentials shifting the electrochemical potential of the QD.

In order to make sure that the QD structure was at the same position throughout, topographic scans of the sample were taken in certain intervals. A drift of the sample holder was not detectable and can therefore be excluded.

[3] If there were more than one set of Coulomb rings observable, the centers of the lower-left set (as in figures 2(c) and (d)) were determined since this is the same set as in the images where only one set is visible. Some Coulomb rings, like those presented in figures 2(c) and (d), are strongly distorted such that their contours could not be fitted with a circle or an ellipse. Therefore, the position of the centers was estimated by eye. The error bars are given by the radius of the innermost Coulomb ring of a given set.

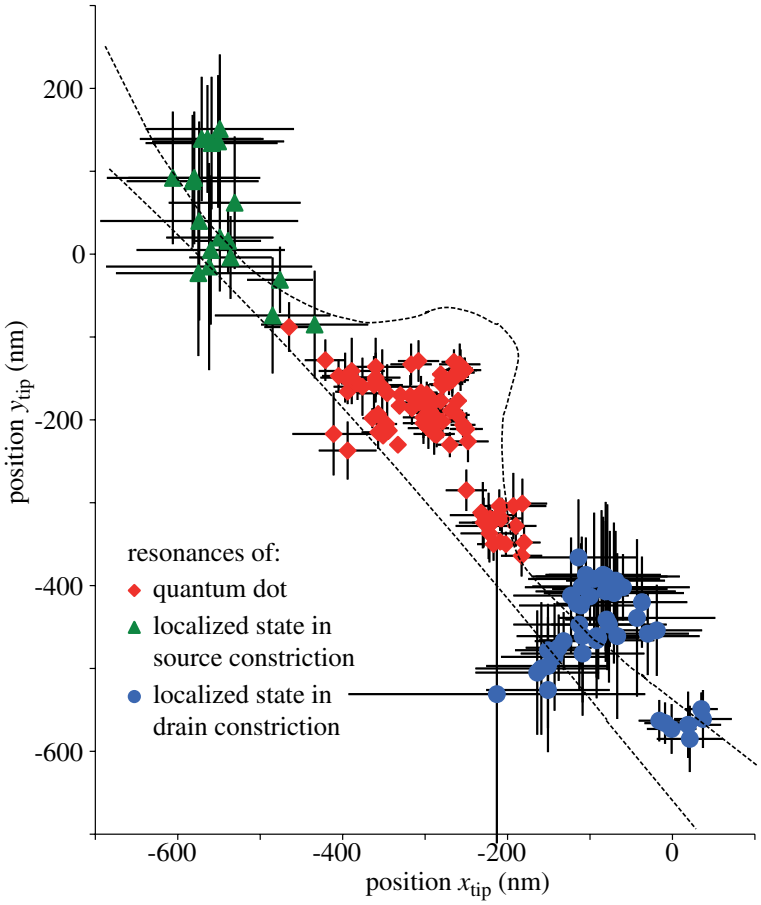

Figure 3. Centers of Coulomb rings of the QD and of the resonances of the localized states in the constrictions plotted in one graph and labeled according to their origin. The position (0,0) corresponds to the center of the scan frame. The lithographic outline of the QD is shown in dashed, black lines. Its position was shifted such that as many centers as possible lie within the QD-boundary [10].

We give a rough estimate of the ratio of the electric force acting on the tip and the mechanical shear force necessary to lead to a deflection of the tip,

$$\frac{F_{\mathrm{el}}}{F_{\mathrm{mech}}} \approx \left.\frac{\mathrm{d}(1/2C(z)U^2)/\mathrm{d}z}{G_{\mathrm{Pt}}\gamma A}\right|_{z=100\,\mathrm{nm}} \sim 10^{-3}.$$

We approximate the tip-sample capacitance $C(z)$ with a plate capacitor with area A which will lead to a drastic overestimation of the energy and hence of the electric force. The tip-sample separation is assumed to be $z = 100\,\mathrm{nm}$ and the tip deflection 400 nm (about the largest shift observed in our measurements) for a rather long tip of 500 μm. This yields a deflection angle of $\gamma = 0.4\,\mu\mathrm{m}/500\,\mu\mathrm{m}$. The shear modulus for platinum, which is a good approximation for our PtIr-tip, is $G_{\mathrm{Pt}} = 6 \times 10^{10}\,\mathrm{Pa}$, and we assume a rather large tip-sample voltage of $U = 10\,\mathrm{V}$. The small ratio of 10^{-3} that is an upper bound clearly indicates that electrostatic forces cannot lead to significant bending of the tip.

Hence, we are left with the third explanation, namely that the shift of Coulomb rings is due to a change in the electrostatic potentials when tuning gates. In fact, when we take a closer look at figure 2, we see that strong voltage differences between gates (especially in (c) and (d)) lead to a significant distortion of the Coulomb rings. This distortion cannot be explained with a drift of the sample holder or bending of the tip. It rather corroborates the importance of electrostatics for the interpretation of SGM images.

The appearance of two sets of Coulomb rings was previously assigned to a double tip [11]. Double-tip behavior can show up in topographic images as double features since a topographic feature, e.g. an edge of a metallic contact, is imaged by each tip individually. The excellent quality of the topographic images (cf figure 1(a)) indicates that we use a sharp, single tip.

In the following, we will present a different explanation that will lead to double features in SGM as observed in figure 2. For a first qualitative understanding, we only consider the tip-dot capacitance $C_{\mathrm{tip}}(x_{\mathrm{tip}})$ and the plunger gate-dot capacitance $C_{\mathrm{PG}}(x_{\mathrm{tip}})$ for tip positions x_{tip} along the (red) arrow in figure 1(a). A plot is shown in figure 1(b). For $x_{\mathrm{tip}} \to \pm\infty$, $C_{\mathrm{tip}} = 0$ and $C_{\mathrm{PG}} = \mathrm{const}$. C_{tip} has a maximum somewhere at the dot position x_{dot}, whereas C_{PG} has a minimum when the tip is located somewhere between the dot position x_{dot} and the gate x_{PG} due to screening by the tip.

Following the constant-interaction model, the electrochemical potential of the QD with N-trapped charge carriers is described by

$$\mu_N(x_{\mathrm{tip}}) = \frac{e^2}{C_\Sigma(x_{\mathrm{tip}})}\left(N - \frac{1}{2}\right) + \frac{C_{\mathrm{tip}}(x_{\mathrm{tip}})}{C_\Sigma(x_{\mathrm{tip}})} e V_{\mathrm{tip}} + \frac{C_{\mathrm{PG}}(x_{\mathrm{tip}})}{C_\Sigma(x_{\mathrm{tip}})} e V_{\mathrm{PG}} + \mathrm{const}, \tag{1}$$

where the total capacitance $C_\Sigma(x_{\mathrm{tip}}) = C_0 - C_{\mathrm{tip}}(x_{\mathrm{tip}}) - C_{\mathrm{PG}}(x_{\mathrm{tip}})$ depends on the tip position x_{tip} and C_{tip}, $C_{\mathrm{PG}} < 0$ are capacitance coefficients. A constant background capacitance C_0 was incorporated into the total capacitance C_Σ. We neglect the single-particle energy since the QD under investigation did not show any signatures of excited states.

Coulomb rings are centered at the extrema of $\mu_N(x_{\mathrm{tip}})$ in an SGM image. We calculate the derivative $\partial\mu_N/\partial x_{\mathrm{tip}}$ of equation (1) and set it to zero. The total capacitance C_Σ depends only weakly on x_{tip} because its value is dominated by the constant background capacitance C_0. Experimental findings [11] and our numerical model below confirm this approximation. Using $\partial C_\Sigma/\partial x_{\mathrm{tip}} \approx 0$, we then find

$$0 = \frac{\partial C_{\mathrm{tip}}(x_{\mathrm{tip}})}{\partial x_{\mathrm{tip}}} V_{\mathrm{tip}} + \frac{\partial C_{\mathrm{PG}}(x_{\mathrm{tip}})}{\partial x_{\mathrm{tip}}} V_{\mathrm{PG}}.$$

This is an implicit equation for the value of x_{tip} where the Coulomb rings are centered. The interpretation of this expression is straightforward with the help of figure 1(b): if the extrema of the two individual capacitances are sufficiently sharp and displaced in space, the equation can be fulfilled for two distinct values of x_{tip} and two sets of Coulomb rings will be observed. Their centers can be shifted by applying different voltages to the tip and the gate.

In the following, we want to extend this qualitative model to a more realistic one in two dimensions based on the real QD structure. The details of the model can be found in the appendix. The spatial dependence of the tip capacitance C_{tip} is assumed to have a Lorentzian shape with an amplitude of 2.4 aF and a width of 600 nm deduced from experimental values. We consider three gates corresponding to the left, plunger and right gate of the real device;

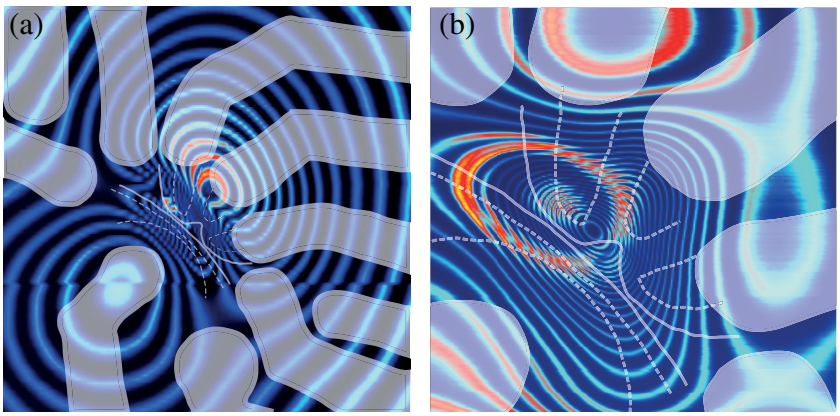

Figure 4. Overlays of the gate-electrode arrangement with SGM images. (a) The total area is $7 \times 7\,\mu\text{m}^2$, and the scanning parameters are $V_{\text{BG}} = 25\,\text{V}$, $V_{\text{tip}} = -1\,\text{V}$, $\Delta z = 200\,\text{nm}$ and $V_{\text{bias}} = 500\,\mu\text{V}$. All other gates are grounded. (b) Zoom into the central area of (a) (area $3 \times 3\,\mu\text{m}^2$) for a different scanning-gate regime ($V_{\text{PG}} = -11.89\,\text{V}$, other parameters as in (a)). A clear spatial correlation between gate electrodes and Coulomb rings is visible in both images; especially (b) demonstrates how Coulomb rings of the tip are 'squeezed' into the electrode-free area.

equation (1) is extended accordingly. Their capacitances to the dot approach a constant value of 4 aF if the tip is placed far away but are screened by the tip for tip positions in the dot-gate region. The precise function is discussed in the appendix. The total capacitance C_Σ also includes a constant background capacitance of 46 aF.

In figures 2(e) and (f), we show the results of a numerical evaluation of the model for two different gate-voltage settings. We plot the contour lines of the electrochemical potential for different integer values N. This is in analogy to the SGM measurement. Our model clearly resembles the measurements presented in panels (c) and (d): we observe at least two sets of Coulomb rings, and their centers can be shifted in real space by applying different gate voltages. If we apply a higher voltage to a particular gate, the corresponding peak in μ_N induced by that gate becomes more pronounced and more Coulomb rings appear. This is also observed in both the measurements and the numerical results.

We see that our model can explain our experimental findings; however, it does not exclude the possibility of the existence of a double tip. Additional support for our model is provided by comparing the scanned resonances with the sample topography: If our argumentation is relevant for our measurements, then we should see a spatial correlation between the gate-electrode arrangement and the appearance of Coulomb rings. In the case that the different sets of Coulomb rings were created by a double or multiple tip, such a correlation would be accidental and is therefore very unlikely. The overlays of the arrangement of the gate electrodes with scanning-gate images in figures 4(a) and (b) show that the pattern of the measured Coulomb rings correlates with the geometry of the device. This is strong evidence that our explanation for the formation of multiple sets of Coulomb rings is relevant for our sample.

4. Comparison with previous scanning-gate microscopy (SGM) experiments, summary

To our knowledge, a strong shift of the centers of Coulomb rings as observed here has not been reported in the literature yet. If more than one set of rings appeared, it was attributed to a double tip [11]. The question remains as to whether previous results have to be re-interpreted in the light of our findings or whether our findings were irrelevant for samples previously investigated. In [1], the authors describe SGM of carbon nanotubes on a back-gated Si-substrate. In fact, the observed Coulomb rings are strongly distorted and resemble the symmetry of the device. This indicates that the gate-electrode arrangement also plays a significant role. This fact is mentioned in the paper but not further discussed.

Most SGM-experiments have been performed on GaAs QDs [7, 11, 12]. The interpretation given there for two sets of Coulomb rings, namely a double tip, seems reasonable since no obvious spatial correlation between SGM images and the topography is observed. The authors do not report any significant shifts, either. In their structures, fabricated using AFM-oxidation techniques, gate voltages do not exceed a few hundred mV's—values which can be exceeded by more than a factor of ten in graphene nanostructures. Consequently, any shifts observed in GaAs will not be as pronounced as in graphene. Moreover, in the case of GaAs-dots, the in-plane gates are formed by the 2DEG. Metallic electrodes contacting the 2DEG are tens of micrometers away from the QD. The GaAs capping layer with a dielectric constant $\varepsilon_{\mathrm{GaAs}} \approx 13$ may further reduce the relevance of mutual screening effects between the tip and the in-plane gates.

SGM was also performed on a superconducting SET [9]. It is interesting to compare this structure to graphene QDs because in both cases the sample is fabricated on a SiO_2-substrate and the metallic gates are very close to the dot and the SET. The SGM images of the SET show a pronounced distortion along the axis connecting the source and drain contacts. This may indicate that mutual screening effects of the tip and the gate electrodes is important for this sample as well. The authors, on the other hand, ascribe the distortion to an asymmetric tip shape. However, the main findings reported in the paper are independent of the detailed interpretation of the distortion.

A fully tunable graphene QD consists of at least five electrodes—source and drain, two gates for tuning the tunnel barriers, and a plunger gate—plus a back gate. The effects described in this paper are intrinsic to a graphene sample and cannot be avoided using more advanced technology. Therefore, it is important to take these effects into account whenever local properties shall be deduced from an SGM image. In principle, it is possible to measure the influence of each individual gate as described in [12] for the tip. Since the contributions to the electrochemical potential are additive, each contribution can be subtracted once determined by measurement. However, this is a tedious task. Additional sets of Coulomb rings and strong shifts of their centers are therefore a phenomenon that probably has to be dealt with again in future scanning-gate experiments, particularly on graphene devices.

Acknowledgments

Financial support by ETH Zürich and the Swiss National Science Foundation are gratefully acknowledged. Some images have been prepared using the WSxM-software [13]. We acknowledge useful discussions with Magdalena Huefner.

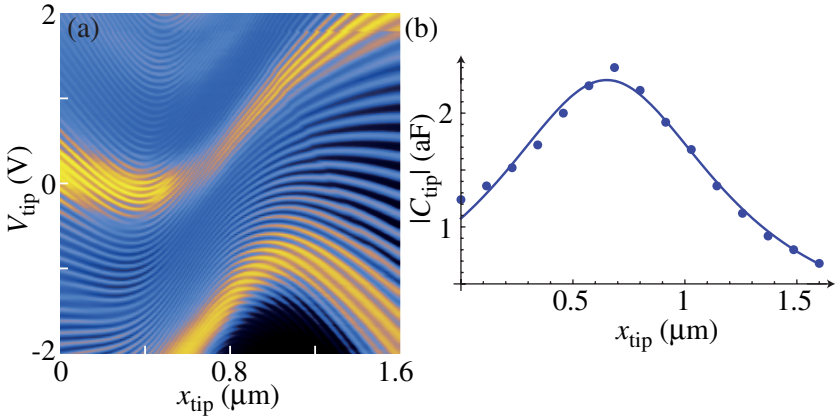

Figure A.1. (a) Sweep of the tip voltage V_{tip} as a function of tip position x_{tip} along a line through the QD. From the spacing of the Coulomb resonances along the V_{tip}-axis, the tip capacitance $C_{tip} = e/\Delta V_{tip}$ as a function of tip position can be deduced, where ΔV_{tip} is the (average) spacing of two Coulomb resonances. In graph (b), the absolute value of the tip capacitance, as measured in (a), is plotted over tip position (blue markers). The line is a fit using a Lorentzian function giving $C_{tip}(x_{tip}) = -2.3\,\text{aF} \times (613\,\text{nm})^2/((x_{tip} - 651\,\text{nm})^2 + (613\,\text{nm})^2)$.

Appendix

In the following, we will describe the electrostatic model that is used to obtain the numerical results presented in the main paper. The tip capacitance is given by a Lorentzian function

$$C_{tip}(\boldsymbol{r}_{tip}) = -2.4\,\text{aF} \times \frac{(600\,\text{nm})^2}{(\boldsymbol{r}_{tip} - \boldsymbol{r}_0)^2 + (600\,\text{nm})^2},$$

where the amplitude and the width is deduced from the measurement shown in figure A.1. We use an offset of $\boldsymbol{r}_0 = -(300\,\text{nm}, 300\,\text{nm})$ in the simulation; this is the position of the QD in the experimental scan frame. The left-gate capacitance is taken to be

$$C_{LG}(\boldsymbol{r}_{tip}) = -\left(4\,\text{aF} - 2.4\,\text{aF} \times \exp\left(-\frac{(x_{tip} - x_{0,LG})^2}{(400\,\text{nm})^2}\right)\right.$$
$$\left.\times \frac{(500\,\text{nm})^2}{((y_{tip} - y_{0,LG}) - (x_{tip} - x_{0,LG})^2/700)^2 + (500\,\text{nm})^2}\right).$$

The first part denotes the constant capacitance for $\boldsymbol{r}_{tip} \to \pm\infty$. The second part is the phenomenological screening term that has an amplitude of 2.4 aF, a lateral decay of the screening effect given by the exponential term with a decay constant of 400 nm, and a Lorentz-like screening term where the rim of the Lorentzian proceeds along a parabola with a coefficient of 1/700. The parameters $x_{0,LG}$ and $y_{0,LG}$ are used to position the gate in space. The plunger and right gates are defined correspondingly with different parameters to position them. They are rotated by 45° and 90°, respectively, to mimic the real device geometry. The total capacitance is then $C_\Sigma(\boldsymbol{r}_{tip}) = 46\,\text{aF} - C_{tip}(\boldsymbol{r}_{tip}) - C_{LG}(\boldsymbol{r}_{tip}) - C_{PG}(\boldsymbol{r}_{tip}) - C_{RG}(\boldsymbol{r}_{tip})$. The constant background capacitance accounts for the measured charging energy of the order of 3 meV that is observed

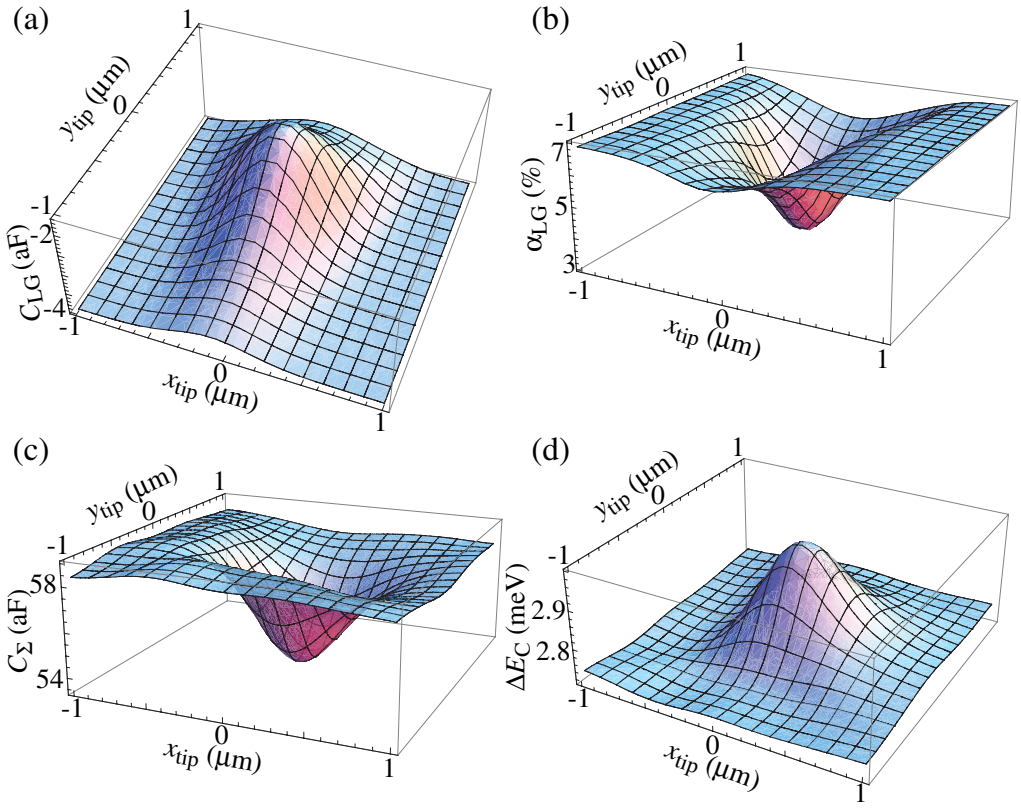

Figure A.2. (a) Left-gate capacitance C_{LG} as a function of tip position as it follows from the above expression. The resulting lever arm α_{LG} is presented in (b). It has a maximum value of below 8%. (c) Total capacitance C_Σ as a function of tip position. As expected, the spatial fluctuations are small compared to the absolute value of the capacitance, namely about 10%. The corresponding charging energy $\Delta E_C = e^2/C_\Sigma$ is shown in (d). Again the fluctuations are about 10% of the absolute value. These values are in good agreement with experimental findings [11]. All images were calculated for an area of $2 \times 2\,\mu\text{m}^2$.

even in the absence of the tip. The electrochemical potential is then given by

$$\mu_N(\boldsymbol{r}_{tip}) = \frac{e^2}{C_\Sigma(\boldsymbol{r}_{tip})}\left(N - \frac{1}{2}\right) + e\frac{C_{tip}(\boldsymbol{r}_{tip})}{C_\Sigma(\boldsymbol{r}_{tip})}V_{tip} + e\frac{C_{PG}(\boldsymbol{r}_{tip})}{C_\Sigma(\boldsymbol{r}_{tip})}V_{PG}$$

$$+e\frac{C_{LG}(\boldsymbol{r}_{tip})}{C_\Sigma(\boldsymbol{r}_{tip})}V_{LG} + e\frac{C_{RG}(\boldsymbol{r}_{tip})}{C_\Sigma(\boldsymbol{r}_{tip})}V_{RG} + \text{const.}$$

With these expressions at hand, it is now possible to calculate the electrostatic influence in our sample numerically and compare them to our experimental findings. In figure A.2, we present the left-gate capacitance C_{LG} in (a), the resulting left-gate lever arm α_{LG} in (b), the total capacitance C_Σ in (c), and the corresponding charging energy ΔE_C in (d). All quantities are plotted for tip positions within an area of $2 \times 2\,\mu\text{m}^2$. The calculated values are in good agreement with experimental findings; in particular the spatial fluctuations of the charging energy of about 10% of its absolute value are confirmed by earlier experiments [11].

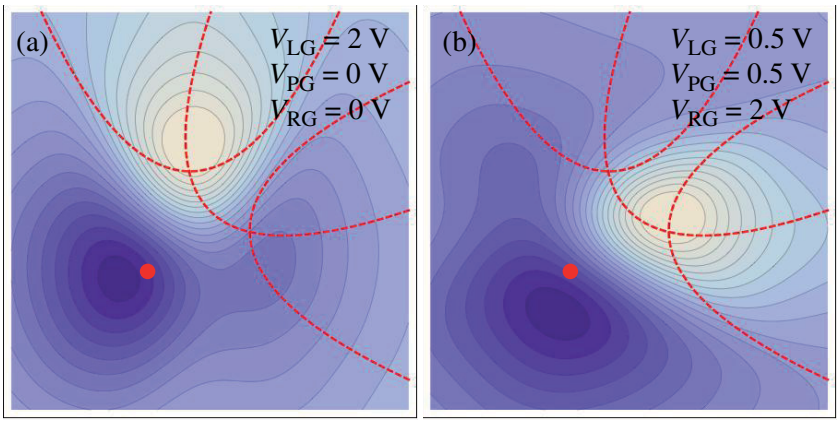

Figure A.3. Numerical simulation of the electrochemical potential of the QD for a fixed number of charge carriers $N = 1$. The QD is located at the (red) circle; the red, dashed parabolas denote the rim along which the screening of the three gates by the tip is strongest. Both images have an area of $2 \times 2\,\mu\text{m}^2$. The gate voltages of the three gates are changed as denoted in the figures and correspond to the values in figures 2(e) and (f). The energy range comprises about 100 meV (brighter colors indicated higher energy) resulting in about 30 Coulomb rings. The tip voltage is $V_{\text{tip}} = 2$ V in both images.

This also justifies the approximation $\nabla_{\boldsymbol{r}_{\text{tip}}} C_\Sigma(\boldsymbol{r}_{\text{tip}}) \approx 0$ in the main paper for the qualitative understanding.

Calculations of the electrochemical potential for a fixed number of charge carriers $N = 1$ are presented in figure A.3. The outline of the geometry, i.e. the parabolas of the gates where the screening by the tip is strongest, is also depicted there with a dashed line. If we vary the number of charge carriers N and determine contour lines of μ_N, we obtain the simulated Coulomb rings shown in figures 2(e) and (f).

References

[1] Woodside M T and McEuen P L 2002 *Science* **296** 1098
[2] Topinka M A, LeRoy B J, Shaw S E J, Heller E J, Westervelt R M, Maranowski K D and Gossard A C 2000 *Science* **289** 2323
[3] Topinka M A, LeRoy B J, Westervelt R M, Shaw S E J, Fleischmann R, Heller E J, Maranowski K D and Gossard A C 2001 *Nature* **410** 183
[4] Pioda A, Kicin S, Brunner D, Ihn T, Sigrist M, Ensslin K, Reinwald M and Wegscheider W 2007 *Phys. Rev.* B **75** 045433
[5] Ihn T, Rychen J, Cilento T, Held R, Ensslin K, Wegscheider W and Bichler M 2002 *Physica* E **12** 691
[6] Hackens B, Martins F, Ouisse T, Sellier H, Bollaert S, Wallart X, Cappy A, Chevrier J, Bayot V and Huant S 2006 *Nat. Phys.* **2** 826
[7] Pioda A, Kicin S, Ihn T, Sigrist M, Fuhrer A, Ensslin K, Weichselbaum A, Ulloa S E, Reinwald M and Wegscheider W 2004 *Phys. Rev. Lett.* **93** 216801
[8] Fallahi P, Bleszyncki A C, Westervelt R M, Huang J, Walls J D, Heller E J, Hanson M and Gossard A C 2005 *Nano Lett.* **5** 223

[9] Huefner M, May C, Kicin S, Ensslin K, Ihn T, Hilke M, Suter K, de Rooij N F and Staufer U 2009 *Phys. Rev.* B **79** 134530
[10] Schnez S, Guettinger J, Huefner M, Stampfer C, Ensslin K and Ihn T 2010 *Phys. Rev.* B **82** 165445
[11] Kicin S, Pioda A, Ihn T, Sigrist M, Fuhrer A, Ensslin K, Reinwald M and Wegscheider W 2005 *New J. Phys.* **7** 185
[12] Gildemeister A E, Ihn T, Sigrist M, Ensslin K, Driscoll D C and Gossard A C 2007 *Phys. Rev.* B **75** 195338
[13] Horcas I, Fernandez R, Gomez-Rodriguez J M, Colchero J, Gomez-Herrero J and Baro A M 2007 *Rev. Sci. Instrum.* **78** 013705